https://doi.org/10.1093/plphys/kiae121 PLANT PHYSIOLOGY 2024: 00: 1–16

Plant Physiology®

Research Article

Triacylglycerol stability limits futile cycles and inhibition of carbon capture in oil-accumulating leaves

Brandon S. Johnson,[1] **Doug K. Allen**,[2,3] **Philip D. Bates**[1,*]

1 Institute of Biological Chemistry, Washington State University, Pullman, WA 99164, USA
2 Donald Danforth Plant Science Center, St. Louis, MO 63132, USA
3 United States Department of Agriculture–Agriculture Research Service, Donald Danforth Plant Science Center, St. Louis, MO 63132, USA

*Author for correspondence: phil_bates@wsu.edu
The author responsible for distribution of materials integral to the findings presented in this article in accordance with the policy described in the Instructions for Authors (https://academic.oup.com/plphys/pages/General-Instructions) is Philip D. Bates.

Abstract

Engineering plant vegetative tissue to accumulate triacylglycerols (TAG, e.g. oil) can increase the amount of oil harvested per acre to levels that exceed current oilseed crops. Engineered tobacco (*Nicotiana tabacum*) lines that accumulate 15% to 30% oil of leaf dry weight resulted in starkly different metabolic phenotypes. In-depth analysis of the leaf lipid accumulation and $^{14}CO_2$ tracking describe metabolic adaptations to the leaf oil engineering. An oil-for-membrane lipid tradeoff in the 15% oil line (referred to as HO) was surprisingly not further exacerbated when lipid production was enhanced to 30% (LEAFY COTYLEDON 2 (LEC2) line). The HO line exhibited a futile cycle that limited TAG yield through exchange with starch, altered carbon flux into various metabolite pools and end products, and suggested interference of the glyoxylate cycle with photorespiration that limited CO_2 assimilation by 50%. In contrast, inclusion of the LEC2 transcription factor in tobacco improved TAG stability, alleviated the TAG-to-starch futile cycle, and recovered CO_2 assimilation and plant growth comparable to wild type but with much higher lipid levels in leaves. Thus, the unstable production of storage reserves and futile cycling limit vegetative oil engineering approaches. The capacity to overcome futile cycles and maintain enhanced stable TAG levels in LEC2 demonstrated the importance of considering unanticipated metabolic adaptations while engineering vegetative oil crops.

Introduction

As world population continues to grow, so do societal needs for energy feedstocks and chemicals obtained from finite supplies of petrochemicals (Singh et al. 2021). An extensive amount of biofuels research is focused on leafy biomass (which is less than 5% lipid; Li-Beisson et al. 2013) and involves the breakdown and fermentation of recalcitrant carbohydrate polymers (Himmel et al. 2007; McCann and Carpita 2015) that is an energetically intensive process. Oleochemicals from natural sources are an alternative that have comparable energy density to petrochemicals and a range of chemical structures for use by the chemical industry (Hill 2007). Oleochemicals derived from plant oils (e.g. triacylglycerols, TAG) are the most energy-rich product of photosynthetic carbon assimilation with over twice the energy density of sugars and can be utilized for food, feed, biofuels, or as feedstocks to the chemical industry for various products such as plastics, polymers, resins, lubricants, etc.; however, production of oil per acre is not comparable to cellulosic levels in plants. Dramatic increases in plant oil production on the same or less arable land are needed to meet the growing global demands. Though most plants accumulate substantial amounts of oil in the seeds or fruit, seed oil accumulation occurs during the last one-third of the plant lifecycle and does not capitalize on available vegetative biomass production. Engineering leafy biomass crops to accumulate energy-dense lipids at oilseed levels would dramatically enhance renewable energy feed stock production.

Received January 11, 2024. Accepted January 26, 2024. Advance access publication March 2, 2024.

Vegetative oil accumulation has been achieved to varied extents (Xu and Shanklin 2016; Vanhercke et al. 2019a), including 4.3% and 8% TAG in sugarcane (*Saccharum* spp. Hybrids) stems and leaves, respectively (Parajuli et al. 2020); 3.3% in potato (*Solanum tuberosum* L.) tubers (Liu et al. 2017); 8.4% in sorghum (*Sorghum bicolor*) (Vanhercke et al. 2019b); 8.7% TAG in leaves of duckweed (*Lemna japonica*) (Liang et al. 2023); 2.5% TAG in perennial ryegrass (*Lolium perenne* L.) (Beechey-Gradwell et al. 2020); and 9% in the leaves of the model plant *Arabidopsis thaliana* (Fan et al. 2014) as a percent of dry weight. None of these compare to that reported in tobacco (*Nicotiana tabacum*) leaves of ∼15% to 30% oil (Vanhercke et al. 2014, 2017). Using a "Push-Pull-Protect" strategy resulted in ∼15% leaf dry weight as TAG (high oil, HO) lines (Vanhercke et al. 2014). The "Push" was generated by expression of the *A. thaliana* WRINKLED1 (WRI1) transcription factor, which increased fatty acid biosynthesis, the *A. thaliana* DIACYLGLYCEROL ACYLTRANSFERASE 1 (DGAT1) provided the "Pull" of acyl groups into TAG, and the oil-body packing protein OLEOSIN (OLE) from sesame (*Sesamum indicum*) provided a hypothetical "Protect" function. The HO lines accumulated 15% dry weight oil but were severely stunted in growth. When the *A. thaliana* LEAFY COTYLEDON 2 (LEC2) transcription factor (a regulator of embryogenesis) under control of the *A. thaliana* SAG12 senescence-inducible promoter was expressed in the HO background, leaf TAG content increased to ∼30% dry weight and surprisingly recovered plant growth near wild-type (WT) level (Vanhercke et al. 2017).

One of the perceived challenges in engineering storage oil production is to avoid compromising essential membrane lipid biosynthesis (Bates 2016) because of substantially overlapping fatty acid biosynthetic and lipid assembly steps. However, the requirement for membranes in leaves presents an opportunity to co-opt some capacity with additional genes or transcription factors to enhance oil storage in vegetative tissues. With fatty acid biosynthesis in the plastid enhanced by AtWRI1 and TAG synthesis by AtDGAT1 in the endoplasmic reticulum of the engineered lines, the required enzymatic steps to produce TAG in leaves are in place (Li-Beisson et al. 2013). Thus, the successful accumulation of lipids in leaves depends on plant metabolism accommodating the engineered increased push and pull of carbon through endogenous metabolic networks into TAG. Understanding how tobacco leaf metabolism adapts to the engineered Push and Pull of carbon into leaf lipids in both the HO and LEC2 lines is a crucial part of the Design–Build–Test–Learn cycle to further enhance lipid metabolism in any species including more productive biomass crops (Pouvreau et al. 2018).

Metabolism is regulated at multiple levels (e.g. transcriptional, translational, post-translational, metabolite activation or inhibition, redox, pH, etc.). Changes in transcripts, proteins, and metabolites can be discordant (Hajduch et al. 2010; Fernie and Stitt 2012; Vogel and Marcotte 2012; Schwender et al. 2014) and may not correspond with flux that is the quantitative cellular phenotype. Thus, measurement of carbon flux is a key complementary approach to global multiomic systems biology analyses to understand the metabolic adjustments associated with genetic engineering. Prior transcriptomic, metabolomic, and lipid specific flux analysis in HO leaves (Vanhercke et al. 2017; Mitchell et al. 2020; Zhou et al. 2020) could not identify the metabolic adjustments associated with vegetative tissue oil biosynthesis, leaving open questions about the effect of the engineering. For example, during HO vegetative growth genes involved in photosynthesis and carbon capture were greatly increased despite the stunted growth of HO. Likewise, the expression of genes involved in fatty acid β-oxidation ether decreased or remained the same in HO as compared to WT, suggesting limited change to fatty acid degradation in the engineered lines during vegetative growth by gene expression analysis alone. Isotopic labeling studies can track altered acyl flux resulting from lipid metabolic engineering and identify endogenous bottlenecks that affect the accumulation of the desired lipid products (Eccleston and Ohlrogge 1998; Bates and Browse 2011; Bates et al. 2014; Yang et al. 2017; Regmi et al. 2020). Previously [^{14}C]acetate tracing of lipid metabolism in isolated leaf disks exposed to constant light indicated that acyl flux in HO was diverted away from photosynthetic membrane production to produce TAG with concomitant increased lipid turnover (Vanhercke et al. 2017; Zhou et al. 2020). Thus, considering the gene expression changes it remained unclear if the enhanced lipid breakdown was partially induced by incubation of excised leaf disks in constant light, and further, what were the consequences of enhanced synthesis/turnover of lipids on carbon partitioning into other metabolic end products such as starch, protein, cell walls, or aqueous-soluble metabolic intermediates. The production and turnover of lipid and starch are crucial to optimal photosynthetic performance and plant growth (Huber and Hanson 1992; Yu et al. 2018; Koper et al. 2021), and the presence of futile cycles wherein starch or lipid are made and turned over and net ATP is consumed, can contribute to changes in growth phenotypes observed in tobacco (Edwards et al. 1999; Baud et al. 2009; Fan et al. 2019; Zhai et al. 2021). $^{14}CO_2$ has been successfully utilized in tobacco to track carbon uptake, source–sink transitions, and partitioning into different metabolic products (Olesinski et al. 1995; Häusler et al. 1998; Oparka et al. 1999). In this study, carbon metabolism in the WT, HO, and LEC2 tobacco lines was traced with $^{14}CO_2$, in planta, to examine the effects of leaf oil engineering on resource partitioning of photosynthetically fixed carbon into various metabolic products.

Results

$^{14}CO_2$ tracing indicates TAG in HO is metabolically dynamic rather than a stable end-product

To understand the effects of the diurnal cycle on lipid production and turnover, 62-d-old WT and HO tobacco plants were pulsed with $^{14}CO_2$ for 1.5 h and allowed to grow for

2 d/night cycles. At the end of the second night, the plants were maintained in the dark for an additional 61 h (Supplementary Fig. S1). The constant dark period was used to assess if leaf TAG turnover may be induced by energy starvation resulting from a lack of light which might occur during harvest and transport of green leaves for biofuel production. The ^{14}C incorporation into total lipids, polar lipids (membrane lipids), and TAG was tracked across the 88 h time course (Supplementary Fig. S1).

WT leaves initially produced more ^{14}C labeled lipids than HO and reached a stable level over the time course; however, total levels of ^{14}C lipids in HO were much more dynamic and decreased over time (Supplementary Fig. S1A). In WT, most of the ^{14}C was associated with membrane lipids and ∼1% in TAG (Supplementary Fig. S1, B and C), consistent with previous leaf labeling and may reflect TAG involvement in leaf lipid homeostasis (Xu and Shanklin 2016; Karki et al. 2019; Zhou et al. 2020). The HO line accumulated less labeled polar lipids and more TAG than WT, suggesting carbon for membrane lipids is re-routed to TAG in HO (Supplementary Fig. S1B), consistent with [^{14}C]acetate labeling of HO leaf disks (Zhou et al. 2020) and indicating good agreement between excised leaf disk and whole plant metabolic labeling experiments. TAG in HO, reached 17% of labeled lipids 3 h after the pulse before declining to 3% to 4% at the end of the chase (Supplementary Fig. S1C), indicating that HO leaves remobilize carbon from TAG. This initial experiment demonstrated the feasibility of utilizing $^{14}CO_2$ to trace differences in carbon metabolism between WT and oil-producing tobacco plants over extended periods; therefore, the approach was extended to analyze more metabolites and include the LEC2 line.

Leaves in mid-development show the greatest differences in oil accumulation

A development study was performed to determine the best stage in plant development for $^{14}CO_2$ metabolic labeling based on: (1) maximal differences in lipid accumulation between WT, HO, and LEC2 lines; and (2) plant size that (a) maximized the available leaf tissue area for sampling and (b) that accommodated the most plants within a 65 L chamber for $^{14}CO_2$ labeling. Total lipid fatty acid content in leaf disks were directly converted to fatty acid methyl esters (FAMEs) and quantified by gas chromatography at 30, 44, and 64 d after sowing (Fig. 1A). The HO plants were smaller than WT while LEC2 plants more closely approached the size of WT (Vanhercke et al. 2017). In the relatively small 30-d plants, the HO leaves accumulated an average of approximately 600 μg FAMEs per leaf disk, nearly 3-fold more lipid content than WT, but not significantly different than LEC2 at this stage. The medium-sized 44-d-old plants had the most significant difference in lipid accumulation between the lines, where LEC2 averaged approximately 900 μg (and

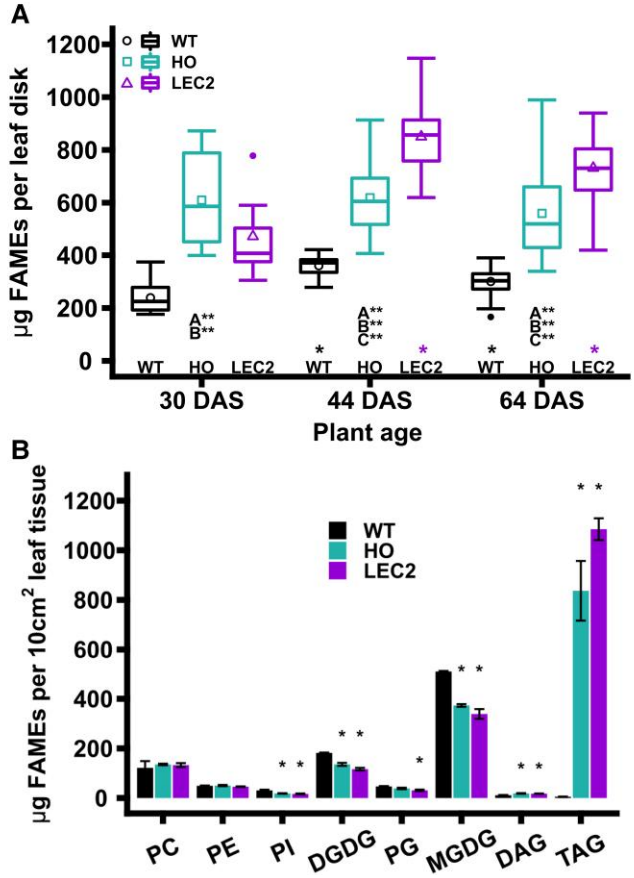

Figure 1. Lipid accumulation in WT, HO, and LEC2 tobacco leaves. **A)** Total leaf lipid accumulation at 30, 44, and 64 DAS. The box represents the interquartile ranges of 25% to 75%, the upper whisker represents the maximum value that is within 1.5 times over the 75th percentile and the lower whisker represents the minimum value that is within 1.5 times under the 25th percentile, the cross bar in the box represents the median, the shape represents the mean, and outliers are points outside of the range of the whiskers (>1.5 times interquartile range). Leaf disks collected (n) during study (30 DAS: $n = 9$ to 18; 44 DAS: $n = 31$ to 54; 64 DAS: $n = 67$ to 107). Significant differences between lines at each age are indicated by comparison, A: WT–HO; B: WT–LEC2; C: HO–LEC2 and significance differences within a line are indicated across the x-axis (reference group = 30 d) (*P-values < 0.05, **P-values < 0.01) were calculated by ANOVA and Tukey Honest Significant Differences test for multiple comparisons. All leaf tissue normalized to 254.5 mm^2. **B)** Glycerolipid analysis for WT and oil-accumulating (HO, LEC2) tobacco. A cork bore (18 mm diameter) was used to collect leaf disks from 40-d-old plants. Five leaf disks were collected from various leaves at random from a single plant and combined for a single sample. Bars represent the mean ($n = 3$, except LEC2 DAG which has $n = 2$) and error bars represent mean ± one standard error. Asterisks above HO and LEC2 bars indicate significant differences (P-value < 0.05) compared to WT (reference group). No significant differences between HO and LEC2. PC, phosphatidylcholine; PE, phosphatidylethanolamine; PI, phosphatidylinositol; PG, phosphatidylglycerol; MGDG, monogalactosyldiacylglycerol; DGDG, digalactosyldiacylglycerol; DAG, diacylglycerol; TAG, triacylglycerol; FAMEs, fatty acid methyl esters.

up to 1,200 μg) FAMEs per leaf disk. While the large 64-d-old plants (similar age to plants in Supplementary Fig. S1) indicated the most oil in the LEC2 lines, they were too large to be used in replicate with the other lines in the 65 L chamber. To confirm that changes in total lipid content of mid-size plants reflected leaf TAG production; we quantified the major neutral and polar lipids (Fig. 1B) and associated fatty acid composition (Supplementary Figs. S2 to S3) in each line from 40-d-old plants. The differences between WT and HO polar lipids and TAG content indicated a large increase in HO TAG content (~12,060%) with a concomitant ~43% decrease in galactolipids relative to WT. The further increase in LEC2 TAG over HO at 40 d after sowing was modestly compensated by an insignificant reduction in mean galactolipid and phosphatidylglycerol content (Fig. 1B). Thus, the LEC2 line greatly increased leaf oil content while maintaining comparable chloroplast membrane content. Based on plant size, leaf area, and differences in lipid accumulation, 40- to 45-d-old plants were chosen for additional $^{14}CO_2$ pulse–chase analysis.

Differential lipid accumulation during a 145 r $^{14}CO_2$ pulse–chase labeling of WT, HO, and LEC2 tobacco

A 2 h $^{14}CO_2$ pulse and chase of 145 h was utilized to analyze the partitioning of photosynthetically fixed carbon into major metabolites between the tobacco lines. Figure 2, A and B demonstrates the labeling chamber and the sampling protocol implemented to minimize differences in individual leaf development between replicate plants and maximize the total leaf area available for sampling. Eight time points were collected across three sequential horizontal leaves on each replicate plant. Two WT replicate plants and three replicate plants of both HO and LEC2 at 45-d-old were able to fit in the 65 L labeling chamber together. At the end of the pulse (designated time 0 h), leaf disks were collected from three sequential leaves per plant ($n = 12$ to 18 at 0 h), and from one leaf per plant at later time points ($n = 4$ to 6) (Fig. 2B). Leaf disk biomass was separated into five major fractions: aqueous soluble metabolites, total protein, cell wall, starch, and total lipids (Fig. 2C). In addition, the lipid fraction was further divided between TAG and polar lipids, and the aqueous fraction was further split out into sugars, organic acids, and amino acids. Plants appeared healthy during the entire experiment and did not show signs of growth defects from sampling (Fig. 2D). The lines varied in lipid accumulation over the 145-h chase time course (Fig. 2E). WT increased lipid mass from 301 to 486 μg FAME per leaf disk over development. At the end of the pulse, leaf disks collected from HO and LEC2 had a similar amount of lipids which was ~1.3- to 1.4-fold greater than WT. Though HO started with more total lipid mass than WT, total FAME per leaf disk in HO only increased slightly from 446 to 500 μg FAME over the 145 h time course. By 100 h after the pulse, total WT lipid mass reached the level of HO and both did not change further over the next 45 h. During the time course, LEC2 lipid mass per leaf disk increased significantly from 406 μg FAME at hour 0 to 1,133 μg FAME at hour 145, an increase of nearly 300% in 7 d. Thus, the plants that were $^{14}CO_2$ labeled grew well and had changes in carbon metabolism leading to differential lipid accumulation over the time course.

Metabolic partitioning of $^{14}CO_2$ into major metabolite fractions differed significantly between lines

At the end of the pulse (Fig. 3A, 0 h), total ^{14}C accumulation indicated significant differences in $^{14}CO_2$ assimilation between each tobacco line. Total ^{14}C, measured as disintegrations per minute (DPM) per leaf area, in WT was over 2-fold greater than HO, and more than 25% greater than LEC2. Total radioactivity decreased over the first 55 h of the chase period before mostly leveling off, indicating partitioning into storage reserves that were less significantly turned over. By 145 h, the total ^{14}C in each line was less than half the value at the end of the pulse (Fig. 3A). The initial decrease in total ^{14}C per leaf area most likely represented the export of photosynthetically fixed carbon from the leaf to other tissues. CO_2 converted into different metabolite fractions was quantified as a percentage of the total radioactivity across the time course (Fig. 3, B to F). The relative proportion of carbon partitioning to aqueous soluble metabolites was not initially significantly different at chase hour 0 between any of the tobacco lines (Fig. 3B), however, the oil accumulating lines had a more rapid efflux of ^{14}C out of the aqueous fraction as the aqueous soluble metabolites were converted to other metabolites during the chase period. By hour 55, WT, HO, and LEC2 were similar in the percentage of ^{14}C in the aqueous fraction and protein (Fig. 3C). At the beginning of the chase, ^{14}C partitioning to the cell wall fraction in HO (21.7%; Fig. 3D) was approximately 1.5-fold greater than WT (14.1%) and more than 1.9-fold greater than LEC2 (11.2%). HO had a higher percent of ^{14}C associated with the cell wall fraction than both WT and LEC2 throughout the experiment, though all lines exhibited similar ^{14}C increases in cell wall over the time course (Fig. 3D). There is no significant difference in the number of cells per leaf area between each line (Supplementary Fig. S4), therefore the increased partition of ^{14}C to HO cell walls, was not due to a higher number of cells per leaf disk.

At the end of the pulse (time 0 h), WT contained significantly more ^{14}C within starch (2.6- to 3.6-fold more) than the HO lines (Fig. 3E, 0 h). Within the first 6 h of the chase, labeled starch increased more rapidly within the oil lines. Then labeled starch decreased in all lines between 6 and 16 h, consistent with starch turnover diurnally. Over the second light period (chase hours 16 to 30) the percent of total ^{14}C in starch increased in all lines; though HO was significantly greater, reaching 18.9% of total ^{14}C, compared to only 7.9% and 10.1% for WT and LEC2, respectively. At the end of the second night (chase hour 40) diurnal starch turnover had resulted in a decrease of ^{14}C starch by approximately 50%.

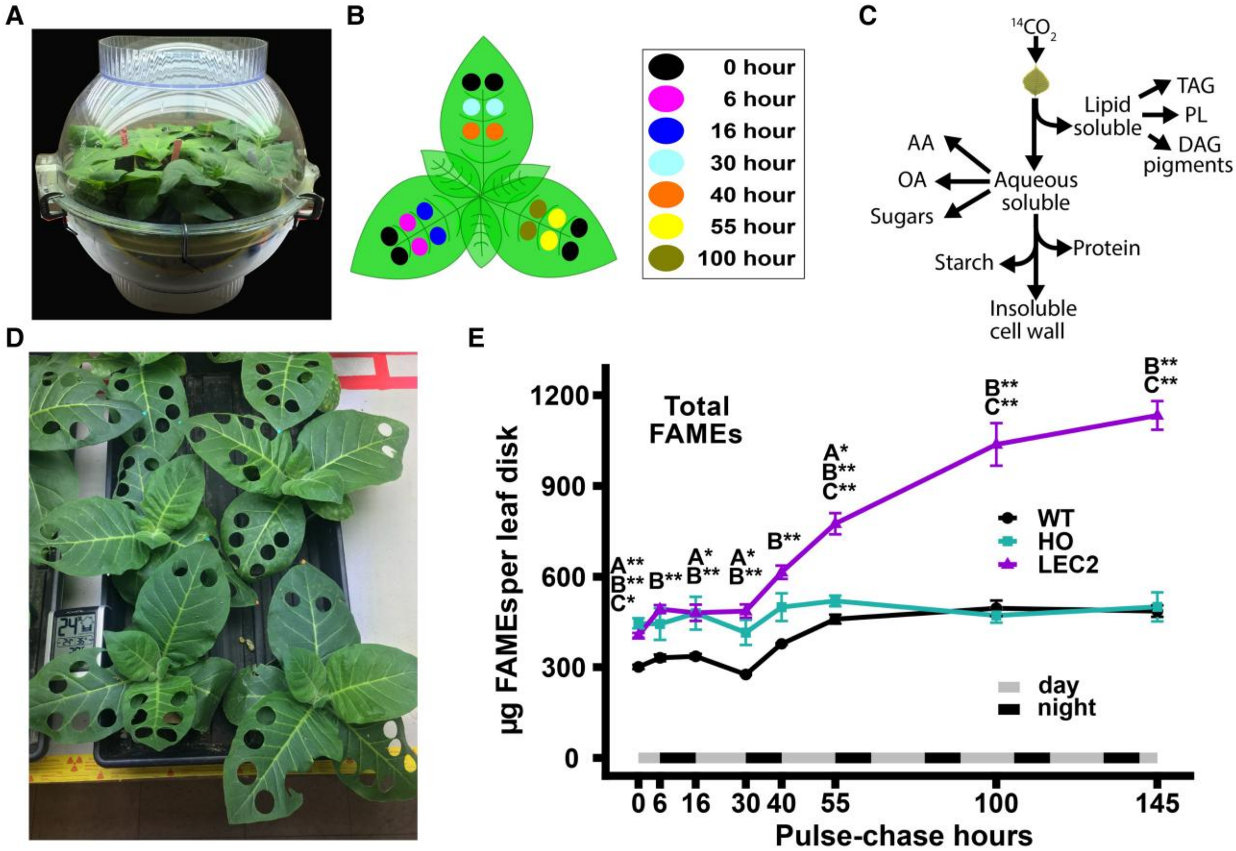

Figure 2. $^{14}CO_2$ pulse–chase experimental design. **A)** Labeling chamber, ∼65 L volume, with two small fans inside to increase circulation of 1 mCi $^{14}CO_2$ during 2-h pulse. **B)** $^{14}CO_2$ pulse–chase sampling protocol: Two WT and three HO and LEC2 plants were sampled at eight time points distributed across three sequential horizontal leaves. Leaf disks were collected from all the leaves at the end of the pulse: 0 h, $n_{(WT)} = 12$, $n_{(HO,\ LEC2)} = 18$ disks. At hours 6 to 100, duplicate leaf disks were collected to represent each leaf number at single time, in an alternating pattern as indicated by colors; $n_{(WT)} = 4$, $n_{(HO,\ LEC2)} = 6$. Hour 145 is not shown in (**B**) since leaf disks were collected randomly where space allowed. Leaf disks were collected by a 14 mm diameter cork bore, ∼154 mm^2 leaf tissue. **C)** Metabolite extraction by sequence of fractionations. **D)** Plants growth during time course. Plants continued growing and appeared healthy after leaf disk collection with the picture taken after the fourth time point (30 h after pulse). **E)** Total lipid mass in leaf disks from the 145 h $^{14}CO_2$ pulse–chase. The unlabeled lipid mass measured as FAMEs from lipid extracts in Fig. 3F. All data points are mean ± SE. Asterisks indicating significant differences between lines, A: WT–HO; B: WT–LEC2; C: HO–LEC2 (ANOVA and Tukey Honest Significant Differences test for multiple comparisons) **P*-value = 0.05 to 0.01, ***P*-value < 0.01.

A dampened increase in labeled starch was also apparent during the third day period (chase hours 40 to 55) and decreased between 55 and 145 h of the chase in all lines. By the end of the chase, HO contained more labeled starch (7.3%) than LEC2 (5.6%) or WT (3.3%), distinct from the end of the pulse (0 h) where WT was 2.6- to 3.6-fold higher than the oil lines.

The partitioning of fixed ^{14}C into total lipids revealed unique differences between each line (Fig. 3F). At hour 0, LEC2 allocated 19.6% of total ^{14}C to lipids, whereas WT and HO were 12.6% and 10.7%, respectively. LEC2 maintained a higher percentage of labeled lipids over both WT and HO until hour 55, when total labeled lipid content on a percent basis was similar in LEC2 and WT and remained so for the duration of the time course. During the first 55 h of the time course, ^{14}C lipid labeling within HO was changing more extensively to offset starch levels and potentially accommodate diurnal carbon needs. By the end of the time course, the fraction of ^{14}C accumulated in HO total lipids was significantly less than WT and LEC2. In summary, total $^{14}CO_2$ uptake was decreased in the oil lines compared to WT, with HO having the largest disparity of less than half the fractional level of lipid relative to WT. LEC2 carbon uptake was measured to be 78.7% of WT, indicating a significant improvement in carbon assimilation relative to HO. Both HO and LEC2 exhibited significant differences in partitioning of fixed ^{14}C from WT and each other, particularly in the cell wall, lipid, and starch fractions indicating metabolic alterations in addition to lipid accumulation in HO and LEC2 lines.

Aqueous metabolite fractions show the greatest differences in organic acid labeling

To further investigate the changes in carbon partitioning between WT and the oil-producing lines, the aqueous

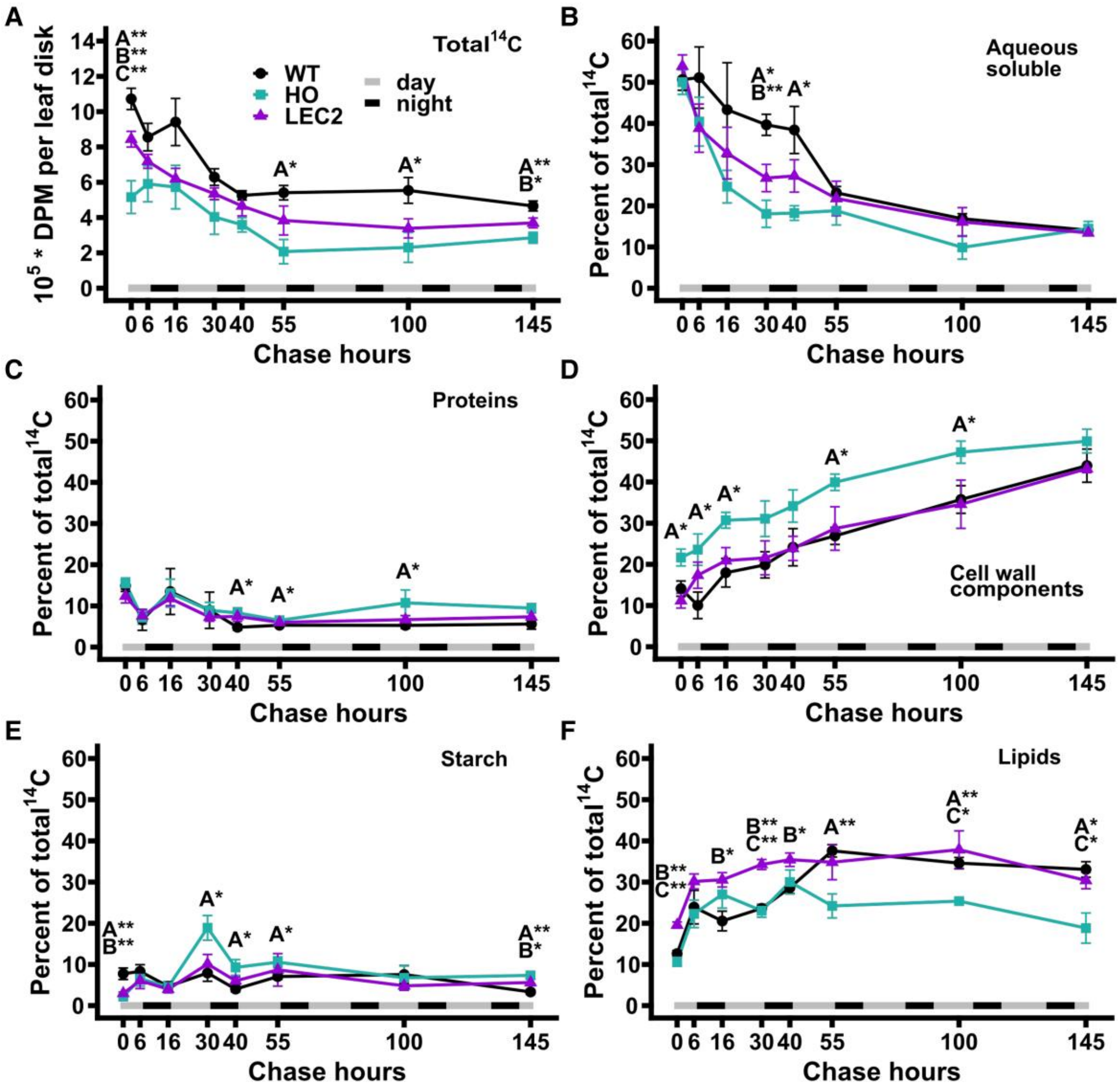

Figure 3. Total radioactivity and label distribution among major metabolite fractions from 145 h $^{14}CO_2$ pulse–chase of 45-d-old WT, HO, and LEC2 lines. Two hour pulse with 1 mCi $^{14}CO_2$, and chase of 145 h. 0 h is the end of the pulse. **A)** Total ^{14}C accumulation in ~ 154 mm^2 leaf disks. **B to F)** Partitioning of ^{14}C to metabolites in the aqueous, protein, cell wall, starch, and lipid phases expressed as a percent of total ^{14}C. Leaf disk collection just prior to lights off and lights on for hours 6, 16, 30, 40, and 55, then every other day for hours 100 and 145. At hour 0, $n_{(WT)} = 12$, $n_{(HO,\ LEC2)} = 18$ disks. At hours 6 to 145, $n_{(WT)} = 4$, $n_{(HO,\ LEC2)} = 6$ disks. For all panels, all data points are mean ± SE. Asterisks indicating significant differences between lines, A: WT–HO; B: WT–LEC2; C: HO–LEC2 (ANOVA and Tukey Honest Significant Differences test for multiple comparisons) **P*-value = 0.05 to 0.01, ***P*-value < 0.01. DPM, disintegrations per minute.

metabolite fraction (Fig. 3B) was split into neutral, anionic, and cationic aqueous metabolite fractions essentially composed of soluble sugars, organic acids, and amino acids, respectively (Fig. 4). At the end of the $^{14}CO_2$ pulse (0 h) the organic acid portion (Fig. 4A) contained more ^{14}C than other aqueous fractions in all lines with WT accumulating the most (30%, 27%, and 18% in WT, LEC2 and HO, respectively) as a percent of total radioactivity (Fig. 4B). The amount of labeled organic acids decreased more rapidly in both oil-producing lines between 0 and 40 chase hours than WT (Fig. 4B), suggesting more rapid turnover of organic acid pools in oil lines than WT, less synthesis of labeled organic acids during the chase period from turnover of other labeled pools in the oil lines, and possibly larger organic acid concentrations in the vacuoles within WT that were labeled. By 55 h into the chase period, the labeled organic acid levels in the WT were similar to the oil lines (Fig. 4B). The percent of total radioactivity in the soluble sugar fraction was similar among the lines and decreased from ~13% to 14% at the end of the pulse (Fig. 4, C and D). The amino acid portion was the least labeled in all lines (Fig. 4E), with percent of total radioactivity in the HO line highest on average and significantly higher than WT at six of the eight time points (Fig. 4F). The free amino acid fraction indicated larger differences between HO and the other two lines (Fig. 4F) than the total protein fraction (Fig. 3C), suggesting that the chase turnover of labeled

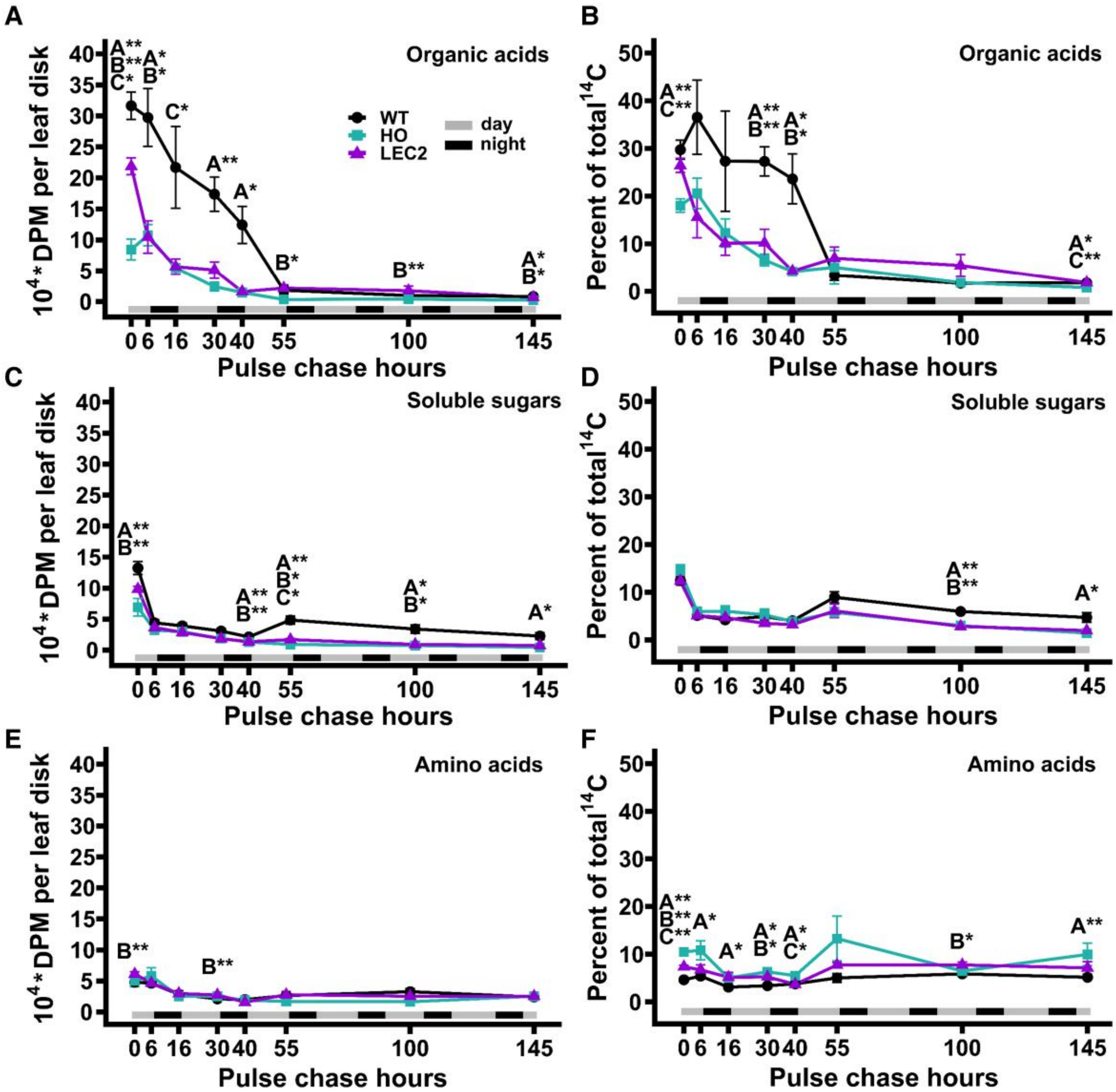

Figure 4. Quantitation of radiolabeled soluble sugars, organic acid, and amino acid fractions from the 145 h $^{14}CO_2$ pulse–chase of WT, HO, and LEC2 tobacco lines. **A, B)** Organic acids, **C, D)** soluble sugars, **E, F)** amino acids fractions expressed as both total radioactivity in each fraction and percent of total radioactivity. For all panels, all data points are mean ± SE. At hour 0, $n_{(WT)} = 12$, $n_{(HO,\ LEC2)} = 18$. At hours 6 to 145, $n_{(WT)} = 4$, $n_{(HO,\ LEC2)} = 6$. Asterisks indicating significant differences between lines, A: WT–HO; B: WT–LEC2; C: HO–LEC2 (ANOVA and Tukey Honest Significant Differences test for multiple comparisons) **P*-value = 0.05 to 0.01, ***P*-value < 0.01. DPM, disintegrations per minute.

metabolites led to a higher flux through free amino acids pools that was not directly involved in protein synthesis.

Distinct patterns of labeled lipid fluxes in each tobacco line

The lipid fraction (Fig. 3F) was separated into neutral lipids and polar lipids by thin-layer chromatography (TLC) and radioactivity in each lipid class was quantified by phosphor imaging (Supplementary Fig. S5). Similar to the initial $^{14}CO_2$ labeling experiment (Supplementary Fig. S1) the WT radiolabeled lipid fraction was predominantly composed of polar lipids (e.g. membrane lipids) (Fig. 5, A, C, and E) with lesser contribution from diacylglycerol (DAG), free sterols, steryl esters, and pigments (Supplementary Fig. S6). TAG represented less than 1% of the labeled lipids in WT (Fig. 5, B, D, and F). The total radioactivity per leaf disk in WT polar lipids reached a maximum at 6 h of the chase and remained roughly constant over the time course (Fig. 5A); though total fixed ^{14}C was decreasing during the same initial period of the chase (Fig. 3A), thus resulting in increased polar lipid percentage as a fraction of total radioactivity of 24.2% (Fig. 5C). When considering the partitioning of ^{14}C within lipids, the label in WT polar lipids was unchanged indicating polar lipid composition was maintained (Fig. 5E). The results indicated that WT membrane lipids synthesized during and shortly after the pulse were stable over the time course.

As expected from the lipid mass quantification (Figs. 1A and 4E) the HO lines both accumulated significantly more ^{14}C-TAG (Fig. 5, B, D, and F) and less labeled polar lipids

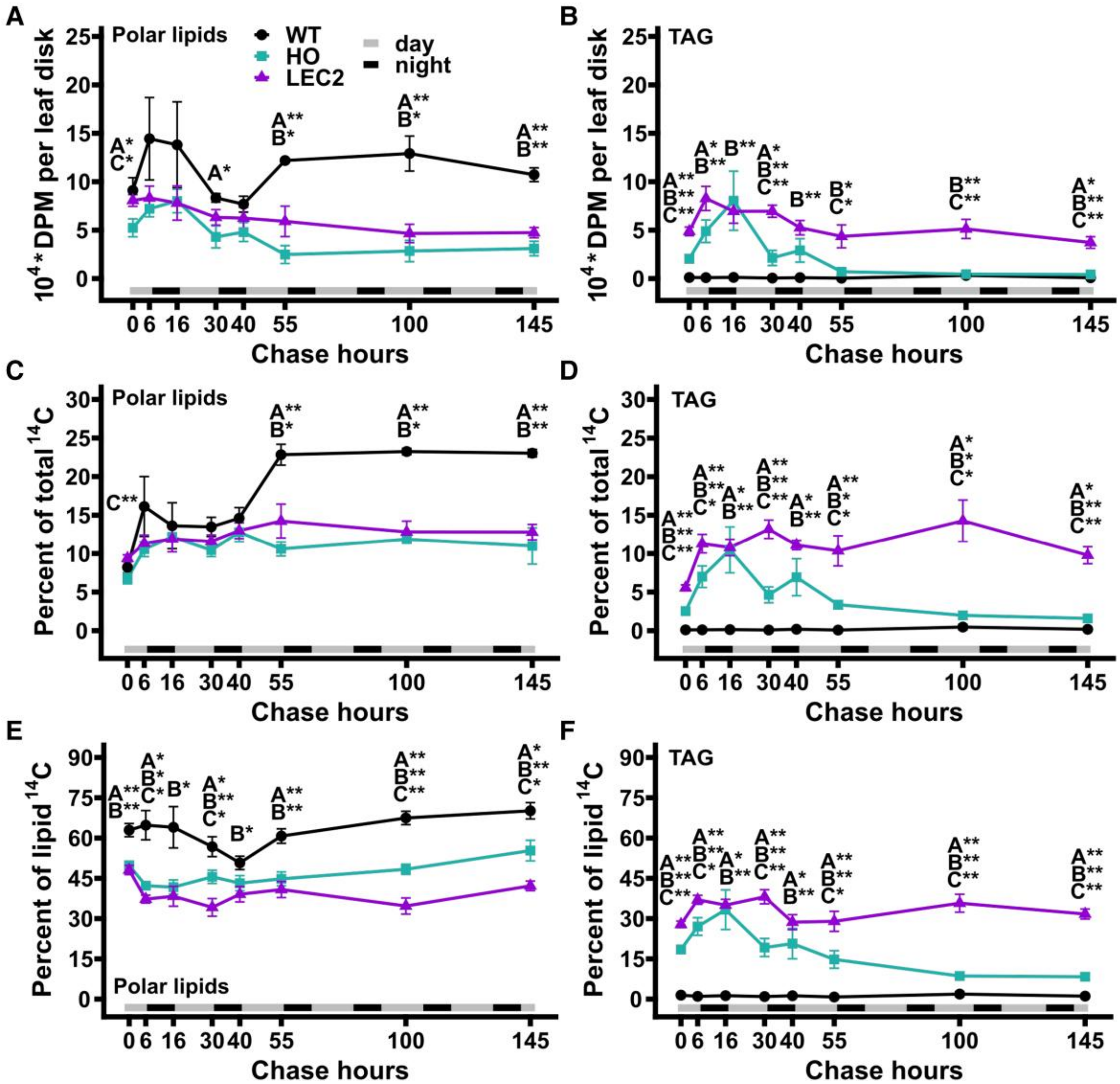

Figure 5. Fractionation and quantitation of radiolabeled lipids from the 145 h $^{14}CO_2$ pulse–chase of WT, HO, and LEC2 tobacco lines. The total lipid extract in Fig. 3F fractionated by TLC into: **A, C, E)** Polar lipids; **B, D,F)** TAG. For all panels, all data points are mean ± SE. At hour 0, $n_{(WT)} = 12$, $n_{(HO, LEC2)} = 18$. At hours 6 to 145, $n_{(WT)} = 4$, $n_{(HO, LEC2)} = 6$. Asterisks indicating significant differences between lines, A: WT–HO; B: WT–LEC2; C: HO–LEC2 (ANOVA and Tukey Honest Significant Differences test for multiple comparisons) *P-value = 0.05 to 0.01, **P-value < 0.01. DPM, disintegrations per minute.

(Fig. 5, A, C, and E) than WT by the end of the pulse. However, each oil line exhibited distinct patterns of ^{14}C lipid flux. In HO, total radioactivity per leaf disk and percent of total ^{14}C for both polar lipids and TAG increased from the end of the pulse through the remaining day and first night (0 to 16 chase hours, Fig. 5, A to D). After 16 h of chase the total ^{14}C per leaf disk for both polar lipids and TAG (Fig. 5, A and B) rapidly decreased during the second day (16 to 30 h), increased slightly during the second night (30 to 40 chase hours), then rapidly decreased again during the third day (40 to 55 chase hours). At 55 h of chase the total ^{14}C per leaf disk in HO polar lipids was about half of the maximum at 16 h, however total ^{14}C in TAG had decreased 94% from the 16 h maximum (Fig. 5, A and B). From 55 to 145 h the remaining total radioactivity in HO polar lipids was stable while TAG continued to decrease (Fig. 5, A and B). As a percent of total fixed ^{14}C (Fig. 3A), the total polar lipid labeling fluctuations were dampened and became near constant from 16 to 145 h (Fig. 5C). However, HO TAG as a percentage of total ^{14}C was similar to the total TAG ^{14}C per leaf disk demonstrating a dynamic pattern (Fig. 5D). The results indicated that labeled TAG in HO was not stable and ^{14}C flux through the TAG pool was dependent on diurnal cycles, with ^{14}C in TAG decreasing during the day and increasing at night. In addition, ^{14}C flux through the HO polar lipid pools only partially mirrored the TAG pool. In LEC2, initial labeling of polar lipids at the end of the pulse was 35% and 43% more than HO as total ^{14}C per leaf disk and percent of total ^{14}C, respectively (Fig. 5, A and C), while LEC2 initial TAG labeling was more than double that of HO by both measures

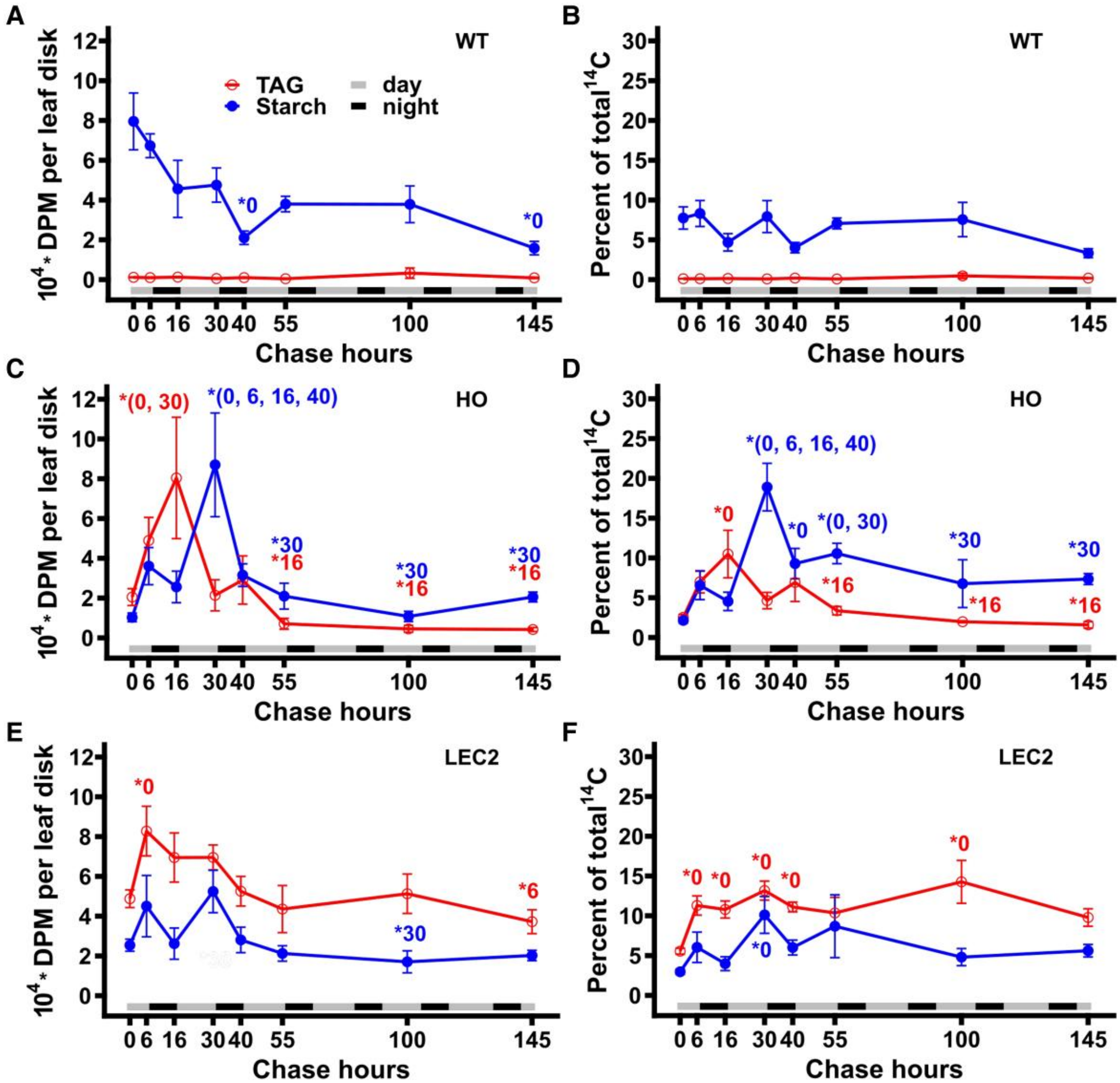

Figure 6. Comparison of radiolabeled TAG and starch from the 145 h $^{14}CO_2$ pulse–chase of WT, HO, and LEC2 tobacco lines. Data obtained from Figs. 4E and 5, B and D and is represented as both total radioactivity in starch (blue) and TAG (red) (**A, C, E**), and as starch and TAG as a percent of total radioactivity (**B, D, F**). A-B, WT. C-D, HO. E-F, LEC2. For all panels, all data points are mean ± SE. At hour 0, $n_{(WT)} = 12$, $n_{(HO,\ LEC2)} = 18$. At hours 6 to 145, $n_{(WT)} = 4$, $n_{(HO,\ LEC2)} = 6$. Asterisks indicating significant differences between lines, A: WT–HO; B: WT–LEC2; C: HO–LEC2 (ANOVA and Tukey Honest Significant Differences test for multiple comparisons) *P-value = 0.05 to 0.01, **P-value < 0.01. DPM, disintegrations per minute.

(Fig. 5, B and D). Total ^{14}C per leaf disk for both polar lipids and TAG of LEC2 reached a maximum by the end of the first day (6 chase hours), and slowly decreased over the time course by 43% and 50%, respectively (Fig. 5, A and B). When considered as a percent of total fixed ^{14}C, both polar lipids and TAG in LEC2 were roughly constant over the time course (Fig. 5, C and D). Together these results indicated that both TAG and membrane lipids were more stable in LEC2 than HO.

Membrane lipids and TAG are produced through a complex metabolic network in which intermediates (e.g. fatty acids, DAG) are exchanged between membrane lipids and TAG (Bates 2016, 2022). Therefore, changes in relative lipid class radioactivity were examined over the pulse–chase period (Fig. 5, E and F). In WT most lipid radioactivity was partitioned into polar lipids with very little in TAG which remained near constant over the time course (Fig. 5E). In both the oil-producing lines the percent of ^{14}C initially incorporated into polar lipids decreased over the first 6 h of chase (Fig. 5E) and was accompanied by an increase in TAG (Fig. 5F) consistent with fatty acids (and possibly DAG) transiently incorporated into PC prior to accumulation in TAG (Bates 2016; Zhou et al. 2020). In HO the percent of total lipid ^{14}C-TAG decreased from 16 to 145 chase hours, and polar lipids increased slightly (Fig. 5, E and F) suggesting the turnover of HO TAG (Fig. 5, B and D) that consequently increases percent polar lipid levels (Fig. 5, A and C) but may also indicate some transfer of ^{14}C from TAG to polar lipids during the chase. In LEC2, the relative labeling of polar lipids and TAG from 6 to 145 h was roughly constant further supporting the stability of TAG in the LEC2 line (Fig. 5, E and F).

LEC2 alleviates a TAG–starch futile cycle present in HO leading to higher TAG content

The relative accumulation of TAG and starch as both total radioactivity (DPM) and percent of total ^{14}C in WT, HO, and LEC2 across the 145 h time course was compared (Fig. 6). At 45 d, diurnal cycling of ^{14}C-starch was apparent in all lines (Fig. 6, A to F); however, the HO line exhibited an inverse pattern of TAG diurnal cycling (Fig. 6, C and D). During the first night (6 to 16 h) labeled starch decreased and labeled TAG increased suggesting the breakdown of starch at night fuels HO TAG biosynthesis. Surprisingly ^{14}C-TAG decreased concomitant with an increase in ^{14}C-starch during the second day (16 to 30 h) indicating the turnover of carbon from TAG to indirectly fuel starch production in HO, which was not apparent in other lines. The pattern repeated though with more dampened response as ^{14}C intermediates of starch and TAG metabolism were siphoned off for other products during the extended chase. While some diurnal cycling of ^{14}C-starch was apparent in LEC2 (Fig. 6, E and F), the amplitude at 16 to 40 h was less than HO, and there was little change in ^{14}C-TAG content. The larger changes in both labeled starch and TAG in HO suggest a TAG-starch futile cycle which was alleviated in the LEC2 line. We hypothesize that examples of turnover may be commonplace in engineered systems that fail to meet expectations; however, evidence for futile cycling requires dynamic labeling as performed here or other data that can be difficult to obtain in practice.

Discussion

In this study, we investigated carbon partitioning in engineered tobacco with ∼15% oil in leaves (HO line), and a second line (LEC2 line) that additionally co-expresses *AtLEC2* in the HO background resulting in increased plant growth and accumulating significantly more oil (∼30% of dry weight) in leaves (Vanhercke et al. 2014, 2017). Through quantitative assessment of the lipid phenotype and isotopic tracing into biomass components and pathway intermediates we demonstrate: (1) TAG within HO leaves can be remobilized out of storage pools during an energy deficit of extended darkness (Supplementary Fig. S1); (2) a period of rapid accumulation of leaf oil in LEC2 leaves from (30 to 44 days after sowing (DAS)) that was absent from HO and is consistent with the delayed expression of the senescence-inducible promoter for *AtLEC2* (Fig. 1A); (3) oil accumulation in HO that coincides with reduced photosynthetic membrane lipid production, but increased TAG content of LEC2 that does not result in additional reductions in photosynthetic membrane lipids (Fig. 1B, Supplementary Figs. S2 and S3); and (4) differences in carbon assimilation and partitioning to lipids, aqueous-soluble, protein, starch, and cell wall components (Figs. 2 to 6) through a quantitative $^{14}CO_2$ pulse–chase labeling design over a ∼7-d period (145 h).

$^{14}CO_2$ labeling indicates differences in carbon assimilation and partitioning between tobacco lines

The $^{14}CO_2$ pulse–chase labeling study revealed that leaves with enhanced TAG accumulation had significant alterations in central carbon metabolism, most prominently in the HO line. The HO line fixed approximately half as much $^{14}CO_2$ as WT and exhibited significantly less ^{14}C partitioned to starch (Fig. 3E, hour 0), more to cell wall (Fig. 3D, hour 0), and increased labeling in the amino acid fraction with concomitant decrease of ^{14}C in the organic acid fraction compared to both WT and LEC2 (Fig. 4, hour 0). ^{14}C in lipids initially did not differ significantly between HO and WT though LEC2 was nearly double the others (Fig. 3F, hour 0). Over the chase period each line had a unique pattern of carbon partitioning as the metabolites labeled during the pulse were converted to downstream products (Figs. 3 to 6). Thus, the effect of the first iteration of leaf oil engineering (i.e. HO line) impacted more than fatty acid synthesis and TAG accumulation, it affected total CO_2 fixation and carbon partitioning with consequences on other aspects of metabolism and biomass production. The inclusion of LEC2 did not further magnify the differential partitioning of HO, but instead partially compensated for the lost carbon assimilation and exhibited metabolism more consistent with WT. The results indicate that engineering leaf metabolism to accumulate oil has a widespread impact on central metabolism, beyond fatty acid synthesis and lipid assembly and may support several intriguing hypotheses.

Hypothesis 1: FA β-oxidation and glyoxylate cycle coinciding with photorespiration in leaf peroxisomes may reduce photorespiratory flux and CO_2 assimilation in HO

The flux of ^{14}C through a TAG–starch futile cycle in HO leaves (Fig. 6, C and D) would involve the mobilization of carbon from TAG through β-oxidation and result in acetyl-CoA that could be used in the glyoxylate cycle or as a precursor of other storage reserves (such as starch through the glyoxylate cycle and gluconeogenesis). In a leaf, the production of glyoxylate occurs substantially through photorespiration (Fig. 7A) (Pan et al. 2020). The additional potential source of glyoxylate may contribute to the observed phenotype. $^{14}CO_2$ enters leaf metabolism through photosynthesis when ribulose 1,5, bisphosphate carboxylase/oxygenase (Rubisco) carboxylates ribulose 1,5 bisphosphate (RBP) that can be metabolically partitioned for fatty acids (Fig. 7A2) and TAG (Fig. 7A3). Photorespiration occurs when Rubisco oxygenates RBP (Fig. 7A1). The pathways of photorespiration (Fig. 7A, purple arrows), β-oxidation (Fig. 7A4), and glyoxylate cycle (Fig. 7A5, 7 to 8) have been extensively characterized and reviewed for many plant species including tobacco (Igamberdiev et al. 1995; Escher and Widmer 1997; Igamberdiev and

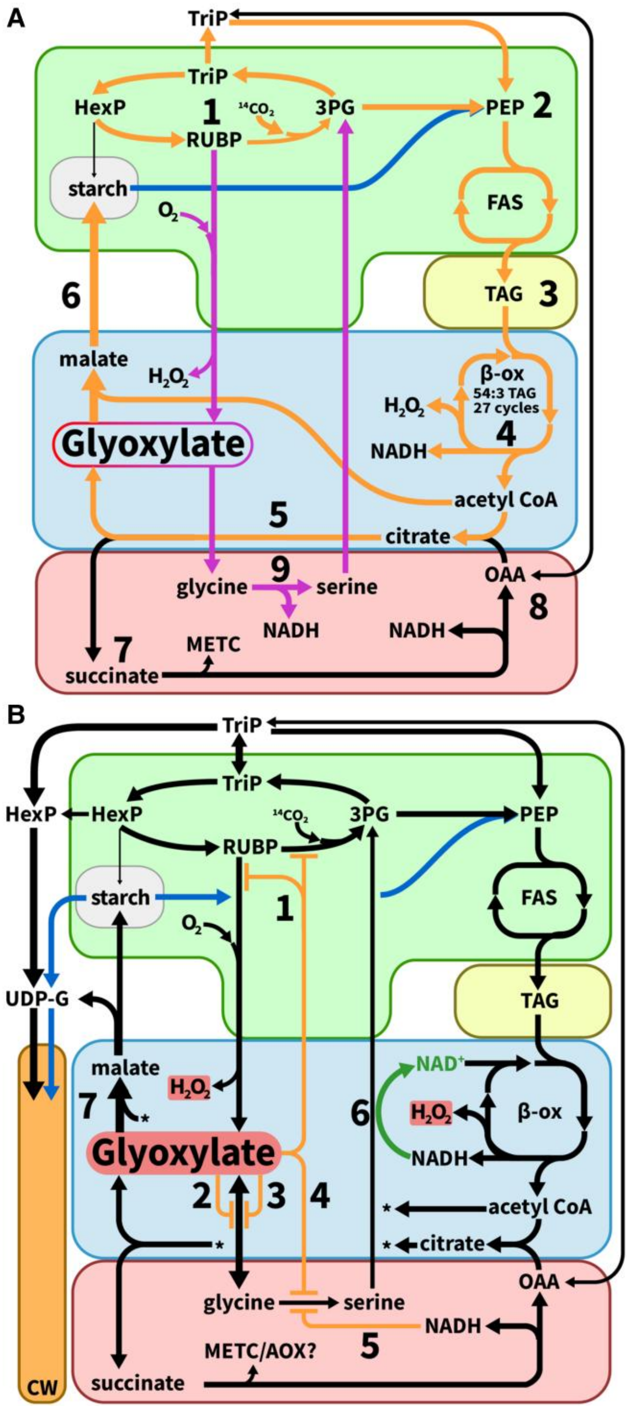

Figure 7. Reorganizing central metabolism to accommodate TAG turnover in tobacco leaves A. TAG–starch futile cycle. Carbon flux through the TAG–starch futile cycle (red and blue arrows) and photorespiration (purple arrows) begins in the chloroplast (green) with (1) photosynthetic carboxylation ($^{14}CO_2$) or oxygenation (O_2) of RUBP, respectively. (2) Calvin cycle partitioning of triose phosphates (triP) to fatty acid synthesis (FAS) is typically cytosolic, though expression analysis suggested a complete plastidial glycolytic pathway may be active to form phosphoenolpyruvate (Vanhercke et al. 2017). New photosynthetic carbon is partitioned to FAS for (3) TAG assembly while (4) β-oxidation degrades TAG that, releases H_2O_2, NADH, and old carbon

(continued)

Kleczkowski 2000; Graham 2008; Bauwe et al. 2010; Tjellström et al. 2015; D'Andrea 2016; Kelly and Feussner 2016; Timm 2020; Timm and Hagemann 2020; Shi and Bloom 2021).

Efficient photorespiratory flux is necessary to maintain carbon assimilation (i.e. autotrophic metabolism) in atmospheric conditions and effectors such as NADH and glyoxylate, both produced within the peroxisome by β-oxidation and glyoxylate cycle, respectively, can inhibit photorespiratory flux (Peterson 1982; Havir 1986; Escher and Widmer 1997; Pritchard et al. 2002; Timm et al. 2012; Lu et al. 2014; Timm et al. 2016; Timm 2020; Timm and Hagemann 2020). High flux through FA β-oxidation and glyoxylate cycle may impair photosynthetic carbon fixation in several ways. Increasing cellular glyoxylate concentration can inhibit enzymes involved in photosynthesis (Rubisco and Rubisco activase, Fig. 7B1) and photorespiration [glutamate:oxoglutarate aminotransferase (GOGAT, Fig. 7B2), serine:glyoxylate aminotransferase (SGAT, Fig. 7B3), glycine decarboxylase complex and serine hyrdroxymethyltransferase (GDC and SHMT, Fig. 7B4)] (Peterson 1982; Havir 1986; Lu et al. 2014). β-Oxidation and regeneration of the glyoxylate cycle substrate oxaloacetate (OAA) from succinate could also elevate cellular redox potential leading to NADH inhibition of GDC in photorespiration (Fig. 7A4, 5, 7 to 9 and B, 1 to 5) (Igamberdiev and Lea 2002; Ma et al. 2016; Igamberdiev and Bykova 2018; Igamberdiev 2020). Further, if GDC were inhibited in the mitochondria, this could result in accumulation of photorespiratory metabolites that modulate Calvin cycle and photorespiration (Fig. 7A9 and B4, 5) (Peterson 1982; Igamberdiev et al. 2004; Timm et al. 2012; Bykova et al. 2014; Negi et al. 2018).

Figure 7. (Continued)
as acetyl-CoA that combines with OAA to form citrate in the glyoxylate cycle within the peroxisome (blue). The glyoxylate cycle converts (5) citrate to glyoxylate and succinate, with the former accepting an acetyl-CoA to form malate and the latter metabolized in the mitochondria (red) (cytosolic *aconitase* reaction step not shown). (6) Malate enters gluconeogenesis in the cytosol and some unknown intermediate is imported to the chloroplast to synthesize starch. (7) Succinate metabolism at complex II increases the redox potential in the mitochondrial electron transport chain during illumination in conjunction with the photosynthetic production of NADPH, while (8) replenishing OAA as the precursor for the glyoxylate cycle. Photorespiratory flux produces glyoxylate and H_2O_2 in the peroxisome and (9) NADH in the mitochondria via glycine decarboxylase complex (GDC). **B)** Inhibition via glyoxylate and NADH of photorespiratory flux stimulates cell wall synthesis. Glyoxylate is a potent inhibitor of (1) Rubisco and Rubisco activase, (2) glutamate:glyoxylate aminotransferase, (3) serine:glyoxylate aminotransferase, and (4) GDC, with GDC also inhibited by NADH (5). Photorespiratory flux to the chloroplast may be enhanced with the reducing potential generated within β-oxidation acting to reduce hydroxypyruvate to glycerate (6). Increased carbon partitioning to the cell wall (orange) in HO (Fig. 3D) may result from the inhibitory effects excess glyoxylate and NADH which redirects carbon flux from photorespiration to gluconeogenesis.

Previous metabolomic and transcriptomic analysis comparing HO to WT (Vanhercke et al. 2017; Mitchell et al. 2020) are mostly consistent with the current metabolic tracing results. The relative abundance of glycine (a downstream product of glyoxylate within photorespiration) was increased nearly 3-fold in HO, while serine (the next metabolic intermediate, Fig. 7A) was not significantly different. Recent reports indicate glycine accumulation as a characteristic marker of alterations in photorespiratory flux (Fu et al. 2023). Therefore, the increase in glyoxylate from β-oxidation could inhibit photorespiration and manifest as increased glycine with inhibition of GDC and SHMT. The increased expression of Rubisco, GDC, SHMT, glutamine synthetase, and hydroxy pyruvate reductase in HO is likely a compensatory mechanism to inhibition by glyoxylate, and together with the altered levels of glycerate and 2-oxoglutarate (Vanhercke et al. 2017; Mitchell et al. 2020) indicate that the balance of photorespiration relative to carbon assimilation has changed and are consistent with altered metabolite and transcript levels of photorespiratory phenotypes previously described (Timm and Bauwe 2013). Though the glyoxylate cycle is normally involved in converting fats to sugars at germination, which is developmentally segregated from photorespiration in leaves, the HO leaves support the combined presence of these pathways that inhibits photorespiration and carbon assimilation, and results in a dramatic reduction in CO_2 fixation and adverse growth phenotypes.

Hypothesis 2: TAG turnover feeds starch synthesis and impairs sink strength leading to reduced CO_2 assimilation in the HO line

The cycling of ^{14}C between TAG and starch in HO (Fig. 6, C and D) suggests carbon from TAG production and turnover is capable of partially offsetting photosynthetically derived starch synthesis (Fig. 7A4 to 6) if enzymatic steps in gluconeogenesis were active. Specifically, the initial limited partitioning of fixed $^{14}CO_2$ to starch in HO (Fig. 6, 0 h) may be a consequence of TAG catabolism during this time (Fig. 7A5 and 6) which would provide an unlabeled source of carbon for starch synthesis. Use of TAG this way could reduce photosynthetic demand for starch, resulting in decreased photosynthetic carbon uptake as has been shown for starchless mutants (Huber and Hanson 1992; Edwards et al. 1999). A starchless *A. thaliana* mutant was improved (i.e. carbon uptake and growth) by directing carbon flux from sugars to lipids and suggests lipids synthesis can be leveraged to increase carbon sink strength (Fan et al. 2019). Furthermore, when lipid storage capacity was enhanced in ryegrass, the authors also observed increased photosynthesis and total carbon content (Beechey-Gradwell et al. 2020). Both studies are similar to the LEC2 line where enhanced fatty acid synthesis and TAG stability (Fig. 5) corresponded with enhanced CO_2 fixation (Fig. 3A). For a system that is producing and turning over starch and fatty acids, net ATP is consumed in the cyclic regeneration of storage reserves, therefore resulting in a futile cycle. The shift in carbon flux to a TAG-starch futile cycle may reflect recently predicted targets of WRI1 in the upper glycolysis and pentose phosphate pathways (Kuczynski et al. 2022) whereby WRI1, also involved in the regulation of cell wall biosynthesis (Haigler et al. 2009; Qu et al. 2012; Qaisar et al. 2017) may account for the unexpected increase of ^{14}C in the HO cell wall (Fig. 3D). These reports support the assertion that altered carbon partitioning and TAG catabolism negatively modulates carbon fixation in photosynthetically active leaves engineered to accumulate lipids. The reassimilation of carbon from TAG turnover into starch biosynthesis reduces the sink strength of starch for photosynthetic carbon to further limit photosynthetic carbon capture.

Hypothesis 3: *AtLEC2* stabilizes TAG accumulation preventing the HO TAG–starch futile cycle and increasing CO_2 assimilation and plant growth

Compared to the first-generation HO tobacco line, the LEC2 accumulated twice as much TAG while mostly alleviating the growth defects of the HO (Vanhercke et al. 2014, 2017). Previously, the metabolic causes for these differential phenotypes were unclear. Here, we demonstrate that the increase in leaf oil accumulation in LEC2 did not come from further diversion of membrane lipids to TAG (Fig. 1), and the enhanced growth was likely associated in part with recovered $^{14}CO_2$ fixation (Fig. 3A). Interestingly partitioning of "new" [^{14}C]carbon to the lipid and TAG fractions increased for LEC2 relative to HO (Figs. 3 and 5) and this increase was attributed to a combination of new carbon partitioning to lipid synthesis and improved TAG stability by reducing TAG degradation in the LEC2 line (Figs. 1 and 5). Recent evidence suggests that co-expressing *LEC2* and *WRI1* promotes TAG synthesis and stability beyond that of *WRI1* alone through enhanced expression of fatty acid synthesis and oil body packing (OLE1/OLE2/OLE3/OLE4/OLE5) (Baud et al. 2007; Kim et al. 2015). We suggest the metabolic stability of TAG in the LEC2 line (Fig. 5) limited the detrimental effects of the TAG–starch futile cycle described in Hypotheses 1 and 2, and thus contributed to the enhanced growth and carbon capture of LEC2 over HO.

Conclusion

The ability to greatly increase the production of plant oils per area of land through the engineering of novel vegetative oil crops holds great potential, but both the amount of oil produced and the effects on plant growth have varied widely in various crop plants (Vanhercke et al. 2019a). Utilizing two previously produced oil accumulating tobacco lines we find that stability of engineered leaf oil accumulation is key to limited adverse metabolic responses in central carbon metabolism (Fig. 7) that otherwise reduce CO_2 assimilation and growth. An inefficient TAG–starch futile cycle in HO that is alleviated in the LEC2 line likely accounts for much of the growth and metabolic differences between the lines. Together with a recent report that tobacco accumulates nontransient starch in leaves which can provide the excess carbon for lipid synthesis (Chu et al. 2022), the results suggest the capacity of tobacco to capture more CO_2 than needed for vegetative growth and store it as a metabolically stable product (nontransient starch, or TAG in LEC2) may account for the success in tobacco leaf oil engineering relative to other species. Interestingly, while the LEC2 is similar to WT in size, $^{14}CO_2$ assimilation was 83.3% of WT suggesting further engineering of the LEC2 line may be able to enhance metabolic performance and further increase leaf oil accumulation.

Materials and methods

Plant growth

Tobacco (*N. tabacum*) seeds were germinated in a growth chamber at 16 h light/8 h dark, 23 °C, and 100 to 300 μmol photons m^{-2} s^{-1} light at pot level (3.5 in. pots). At 30 DAS, plants were transferred to 2.8-L pots in a greenhouse with supplemental lighting and heating set to 16 h light/8 h dark, 28/20 °C, and 200 to 400 μmol photons m^{-2} s^{-1}. Watered daily, as needed, and fertilized twice per week with 20/10/20 NPK (1 part fertilizer:15 parts water) with an additional 200 ppm micronutrient solution of Scotts Miracle-Gro.

Leaf lipid mass measurements

Three plants utilized per genotype for total fatty acid analysis, 7 mm diameter leaf disks were collected from 1 to 3 leaves at 30 DAS, 16 mm disks were collected from four to six leaves at 44 DAS, and from five to seven leaves at 64 DAS. Disks were submerged in 1.5 mL 2.5% sulfuric acid in methanol (v/v) in glass tubes containing 17:0 TAG standard and incubated at 80 °C for 1 h to produce FAME. 0.5 mL hexanes and 3 mL 0.9% KCl (w/v) was added to induce phase separation. FAME in the upper hexanes phase concentrated under N_2 and re-suspended in 0.2 mL hexanes for quantification via gas chromatography with flame ionization detection (GC-FID) on Restek FATwax column (30 m, 0.25 inner diameter, 0.25 mm film thickness). Five microliters injection, 1/40 split ratio, 0.9 mL/min helium flow rate. Heating conditions: 170 °C ramped 10 °C per minute to 230 °C, hold 5 min. FAME data was normalized to a leaf disk area. For lipid class analysis, lipid extraction and TLC were done as previously (Zhou et al. 2020). Lipid classes identified by TLC migration with standards after staining with 0.05% (w/v) primulin in acetone/water 80:20 (v/v) and visualized under UV light, then removed from TLC for conversion to FAME and analyzed by GC-FID.

14CO_2 pulse chase

35-DAS plants were transferred to the lab for 10 d to acclimate to environmental conditions of ~350 μmol photons m^{-2} s^{-1} of fluorescent light at 22 to 30 °C and ~20% to 30% humidity. The 45-d-old tobacco plants (2 WT, 3 HO, 3 LEC2) were placed together in a 65 L desiccator under the lights containing two small fans, and a vial of 1 mCi [^{14}C]bicarbonate (American Radiolabeled Chemicals, Inc). The 2 h pulse (evolution of $^{14}CO_2$) was triggered by delivering 2 mL of 5 M sulfuric acid to the [^{14}C]bicarbonate via tubing and syringe at 5 h into the day. At the end of the pulse the chamber was purged inside a fume hood through a 1 M KOH base trap to capture any remaining $^{14}CO_2$. Once removed the plants were placed under lights and the 0 h leaf disks were collected from the first three sequential leaves above the cotyledons near the tip (12-WT, 18-HO, 18-LEC2 replicates). T for subsequent time points, two disks were collected from each side of the midrib moving toward the base 4-WT, 6-HO, 6-LEC2 replicates (Fig. 2A). All leaf disks were immediately frozen in liquid N_2 and stored at −80 °C.

Extraction and analysis of ^{14}C fractions

All solvents and tools were stored at −20 °C or on ice until use. Leaf disks were homogenized by bead beater in 2 mL tubes with five 2.4 mm ceramic beads for three to four intervals of 30 s on medium speed. After each interval, samples were frozen in liquid nitrogen for 20 s. The extraction of lipids, organic acids, amino acids, sugars, protein, starch, and cell wall was as in (Allen and Young 2013) except for modifications of chloroform/methanol/1 M formic acid (20/10/1; v/v/v) for lipid extraction solvent, and a 3 h Solusol (National Diagnostics) digestion to dissolve the cell wall fraction. Radioactivity in aliquots of each fraction was quantified with a Packard Tri-Carb 2,200 scintillation counter and data analyzed with Microsoft Excel and R. An aliquot of the labeled lipid fraction was also used to measure total mass by GC-FID of FAME and individual lipid classes by TLC as above.

Statistical analysis

All statistical tests were performed with the programming language R (version 4.3.1) (R Core Team 2023) for Windows.

Supplementary data

The following materials are available in the online version of this article.

Supplementary Figure S1. $^{14}CO_2$ pulse–chase tracing of lipid metabolism in 62-d-old WT and HO leaves under day night cycles and constant darkness.

Supplementary Figure S2. Fatty acid composition (micrograms per 10 cm^2 leaf area) of glycerolipids for WT and oil-accumulating (HO, LEC2) tobacco (Fig. 1B).

Supplementary Figure S3. Fatty acid composition (percent of glycerolipid mass) of lipids for WT and oil-accumulating (HO, LEC2) tobacco (Fig. 1B).

Supplementary Figure S4. Cell counts of leaf pavement cells from 45-d-old WT, HO, and LEC2 tobacco at 20× magnification.

Supplementary Figure S5. Total lipid extract visualized after TLC in hexane/diethyl ether/acetic acid (70/30/1, v/v/v).

Supplementary Figure S6. Minor lipid fractions from the 145 h $^{14}CO_2$ pulse–chase of WT, HO, and LEC2 tobacco lines.

Acknowledgments

We thank Xue-Rong Zhou of CSIRO, Australia for providing the transgenic tobacco lines.

Author contributions

P.D.B. and D.K.A. conceived the original research plans and acquired the funding; B.S.J. performed the experiments; all authors analyzed the data and contributed to writing the article.

Funding

This material is based upon work supported by the United States Department of Agriculture National Institute of Food and Agriculture #2017-67013-29481 and #2021-67013-33778, the Hatch Umbrella Project #1015621, the Multi-State Project #NC1203, the National Science Foundation (#PGRP-IOS-1829365), and the U. S. Department of Energy, Office of Science, Office of Biological and Environmental Research, under award number DE-SC0023142. Additionally, the authors acknowledge support from the United States Department of Agriculture–Agricultural Research Service and the Donald Danforth Plant Science Center.

Conflict of interest statement. None declared.

Data availability

The data underlying this article are available in the article and in its online supplementary material.

References

Allen DK, Young JD. Carbon and nitrogen provisions alter the metabolic flux in developing soybean embryos. Plant Physiol. 2013:**161**(3):1458–1475. https://doi.org/10.1104/pp.112.203299

Bates PD. Understanding the control of acyl flux through the lipid metabolic network of plant oil biosynthesis. Biochim Biophys Acta. 2016:**1861**(9):1214–1225. https://doi.org/10.1016/j.bbalip.2016.03.021

Bates PD. Chapter Six - The plant lipid metabolic network for assembly of diverse triacylglycerol molecular species, Advances in Botanical Research. Vol. 101. Academic Press; 2022. p. 225–252. https://doi.org/10.1016/bs.abr.2021.07.003

Bates PD, Browse J. The pathway of triacylglycerol synthesis through phosphatidylcholine in Arabidopsis produces a bottleneck for the accumulation of unusual fatty acids in transgenic seeds. Plant J. 2011:**68**(3):387–399. https://doi.org/10.1111/j.1365-313X.2011.04693.x

Bates PD, Johnson SR, Cao X, Li J, Nam J-W, Jaworski JG, Ohlrogge JB, Browse J. Fatty acid synthesis is inhibited by inefficient utilization of unusual fatty acids for glycerolipid assembly. Proc Natl Acad Sci USA. 2014:**111**(3):1204–1209. https://doi.org/10.1073/pnas.1318511111

Baud S, Mendoza MS, To A, Harscoët E, Lepiniec L, Dubreucq B. WRINKLED1 specifies the regulatory action of LEAFY COTYLEDON2 towards fatty acid metabolism during seed maturation in Arabidopsis. Plant J. 2007:**50**(5):825–838. https://doi.org/10.1111/j.1365-313X.2007.03092.x

Baud SB, Wuillème S, To A, Rochat C, Lepiniec LC. Role of WRINKLED1 in the transcriptional regulation of glycolytic and fatty acid biosynthetic genes in Arabidopsis. Plant J. 2009:**60**(6):933–947. https://doi.org/10.1111/j.1365-313X.2009.04011.x

Bauwe H, Hagemann M, Fernie AR. Photorespiration: players, partners and origin. Trends Plant Sci. 2010:**15**(6):330–336. https://doi.org/10.1016/j.tplants.2010.03.006

Beechey-Gradwell Z, Cooney L, Winichayakul S, Andrews M, Hea SY, Crowther T, Roberts N. Storing carbon in leaf lipid sinks enhances perennial ryegrass carbon capture especially under high N and elevated CO2. J Exp Bot. 2020:**71**(7):2351–2361. https://doi.org/10.1093/jxb/erz494

Bykova NV, Møller IM, Gardeström P, Igamberdiev AU. The function of glycine decarboxylase complex is optimized to maintain high photorespiratory flux via buffering of its reaction products. Mitochondrion. 2014:**19**:357–364. https://doi.org/10.1016/j.mito.2014.01.001

Chu KL, Koley S, Jenkins LM, Bailey SR, Kambhampati S, Foley K, Arp JJ, Morley SA, Czymmek KJ, Bates PD, et al. Metabolic flux analysis of the non-transitory starch tradeoff for lipid production in mature tobacco leaves. Metab Eng. 2022:**69**:231–248. https://doi.org/10.1016/j.ymben.2021.12.003

D'Andrea S. Lipid droplet mobilization: the different ways to loosen the purse strings. Biochimie. 2016:**120**:17–27. https://doi.org/10.1016/j.biochi.2015.07.010

Eccleston VS, Ohlrogge JB. Expression of lauroyl-acyl carrier protein thioesterase in Brassica napus seeds induces pathways for both fatty acid oxidation and biosynthesis and implies a set point for triacylglycerol accumulation. Plant Cell. 1998:**10**(4):613–621. https://doi.org/10.1105/tpc.10.4.613

Edwards JS, Thomas WO, Gerald E. Modification of carbon partitioning, photosynthetic capacity, and O2 sensitivity in Arabidopsis plants with low ADP-glucose pyrophosphorylase activity. Plant Physiol. 1999:**119**(1):267–276. https://doi.org/10.1104/pp.119.1.267

Escher C-L, Widmer F. Lipid mobilization and gluconeogenesis in plants: do glyoxylate cycle enzyme activities constitute a real cycle? a hypothesis. Biol Chem. 1997:**378**:803–813.

Fan J, Yan C, Roston R, Shanklin J, Xu C. Arabidopsis lipins, PDAT1 acyltransferase, and SDP1 triacylglycerol lipase synergistically direct fatty acids toward beta-oxidation, thereby maintaining membrane lipid homeostasis. Plant Cell. 2014:**26**(10):4119–4134. https://doi.org/10.1105/tpc.114.130377

Fan J, Zhou C, Yu L, Li P, Shanklin J, Xu C. Diversion of carbon flux from sugars to lipids improves the growth of an Arabidopsis starchless mutant. Plants. 2019:**8**(7):229. https://doi.org/10.3390/plants8070229

Fernie AR, Stitt M. On the discordance of metabolomics with proteomics and transcriptomics: coping with increasing complexity in logic, chemistry, and network interactions scientific correspondence. Plant Physiol. 2012:**158**(3):1139–1145. https://doi.org/10.1104/pp.112.193235

Fu X, Gregory LM, Weise SE, Walker BJ. Integrated flux and pool size analysis in plant central metabolism reveals unique roles of glycine and serine during photorespiration. Nat Plants. 2023:**9**(1):169–178. https://doi.org/10.1038/s41477-022-01294-9

Graham IA. Seed storage oil mobilization. Annu Rev Plant Biol. 2008:**59**(1):115–142. https://doi.org/10.1146/annurev.arplant.59.032607.092938

Haigler CH, Singh B, Wang G, Zhang D. Genomics of cotton fiber secondary wall deposition and cellulose biogenesis. Genetics and genomics of cotton. US: Springer; 2009. p. 385–417.

Hajduch M, Hearne LB, Miernyk JA, Casteel JE, Joshi T, Agrawal GK, Song Z, Zhou M, Xu D, Thelen JJ. Systems analysis of seed filling in Arabidopsis: using general linear modeling to assess concordance of transcript and protein expression. Plant Physiol. 2010:**152**(4):2078–2087. https://doi.org/10.1104/pp.109.152413

Häusler RE, Schlieben NH, Schulz B, Flügge U-I. Compensation of decreased triose phosphate/phosphate translocator activity by accelerated starch turnover and glucose transport in transgenic tobacco. Planta. 1998:**204**(3):366–376. https://doi.org/10.1007/s004250050268

Havir EA. Inactivation of serine:glyoxylate and glutamate:glyoxylate aminotransferases from tobacco leaves by glyoxylate in the presence of ammonium Ion. Plant Physiol. 1986:**80**(2):473–478. https://doi.org/10.1104/pp.80.2.473

Hill K. Industrial development and application of biobased oleochemicals. Pure Appl Chem. 2007:**79**(11):1999–2011. https://doi.org/10.1351/pac200779111999

Himmel ME, Ding S-Y, Johnson DK, Adney WS, Nimlos MR, Brady JW, Foust TD. Biomass recalcitrance: engineering plants and enzymes for biofuels production. Science. 2007:**315**(5813):804–807. https://doi.org/10.1126/science.1137016

Huber SC, Hanson KR. Carbon partitioning and growth of a starchless mutant of Nicotiana sylvestris. Plant Physiol. 1992:**99**(4):1449–1454. https://doi.org/10.1104/pp.99.4.1449

Igamberdiev AU. Citrate valve integrates mitochondria into photosynthetic metabolism. Mitochondrion. 2020:**52**:218–230. https://doi.org/10.1016/j.mito.2020.04.003

Igamberdiev AU, Bykova NV. Role of organic acids in the integration of cellular redox metabolism and mediation of redox signalling in photosynthetic tissues of higher plants. Free Radic Biol Med. 2018:**122**:74–85. https://doi.org/10.1016/j.freeradbiomed.2018.01.016

Igamberdiev AU, Kleczkowski LA. Capacity for NADPH/NADP turnover in the cytosol of barley seed endosperm: the role of NADPH-dependent hydroxypyruvate reductase. Plant Physiol Biochem. 2000:**38**(10):747–753. https://doi.org/10.1016/S0981-9428(00)01187-6

Igamberdiev AU, Lea PJ. The role of peroxisomes in the integration of metabolism and evolutionary diversity of photosynthetic organisms. Phytochemistry. 2002:**60**(7):651–674. https://doi.org/10.1016/S0031-9422(02)00179-6

Igamberdiev AU, Mikkelsen TN, Ambus P, Bauwe H, Lea PJ, Gardeström P. Photorespiration contributes to stomatal regulation and carbon isotope fractionation: a study with barley, potato and Arabidopsis plants deficient in Glycine decarboxylase. Photosyn Res. 2004:**81**(2):139–152. https://doi.org/10.1023/B:PRES.0000035026.05237.ec

Igamberdiev AU, Popov VN, Falaleeva MI. Alternative system of succinate oxidation in glyoxysomes of higher plants. FEBS Lett. 1995:**367**(3):287–290. https://doi.org/10.1016/0014-5793(95)00563-O

Karki N, Johnson BS, Bates PD. Metabolically distinct pools of phosphatidylcholine are involved in trafficking of fatty acids out of and into the chloroplast for membrane production. Plant Cell. 2019:**31**(11):2768–2788. https://doi.org/10.1105/tpc.19.00121

Kelly AA, Feussner I. Oil is on the agenda: lipid turnover in higher plants. Biochim Biophys Acta. 2016:**1861**(9):1253–1268. https://doi.org/10.1016/j.bbalip.2016.04.021

Kim HU, Lee K-R, Jung S-J, Shin HA, Go YS, Suh M-C, Kim JB. Senescence-inducible LEC2 enhances triacylglycerol accumulation in leaves without negatively affecting plant growth. Plant Biotechnol J. 2015:**13**(9):1346–1359. https://doi.org/10.1111/pbi.12354

Koper K, Hwang S-K, Singh S, Okita TW. Source-sink relationships and its effect on plant productivity: manipulation of primary carbon and starch metabolism. Genome Eng Crop Improv. 2021:1–31.

Kuczynski C, McCorkle S, Keereetaweep J, Shanklin J, Schwender J. An expanded role for the transcription factor WRINKLED1 in the biosynthesis of triacylglycerols during seed development. Front Plant Sci. 2022:**13**:955589. https://doi.org/10.3389/fpls.2022.955589

Li-Beisson Y, Shorrosh B, Beisson F, Andersson MX, Arondel V, Bates PD, Baud S, Bird D, Debono A, Durrett TP, et al. Acyl-lipid metabolism. Arabidopsis Book. 2013:**11**:e0161. https://doi.org/10.1199/tab.0161

Liang Y, Yu XH, Anaokar S, Shi H, Dahl WB, Cai Y, Luo G, Chai J, Cai Y, Molla-Morales A, et al. Engineering triacylglycerol accumulation in duckweed (Lemna japonica). Plant Biotechnol J. 2023:**21**(2):317–330. https://doi.org/10.1111/pbi.13943

Liu Q, Guo Q, Akbar S, Zhi Y, El Tahchy A, Mitchell M, Li Z, Shrestha P, Vanhercke T, Ral J-P, et al. Genetic enhancement of oil content in potato tuber (Solanum tuberosum L.) through an integrated metabolic engineering strategy. Plant Biotechnol J. 2017:**15**(1):56–67. https://doi.org/10.1111/pbi.12590

Lu Y, Li Y, Yang Q, Zhang Z, Chen Y, Zhang S, Peng X-X. Suppression of glycolate oxidase causes glyoxylate accumulation that inhibits photosynthesis through deactivating Rubisco in rice. Physiol Plant. 2014:**150**(3):463–476. https://doi.org/10.1111/ppl.12104

Ma Z, Marsolais F, Bernards MA, Sumarah MW, Bykova NV, Igamberdiev AU. Glyoxylate cycle and metabolism of organic acids in the scutellum of barley seeds during germination. Plant Sci. 2016:**248**:37–44. https://doi.org/10.1016/j.plantsci.2016.04.007

McCann MC, Carpita NC. Biomass recalcitrance: a multi-scale, multi-factor, and conversion-specific property. J Exp Bot. 2015:**66**(14):4109–4118. https://doi.org/10.1093/jxb/erv267

Mitchell MC, Pritchard J, Okada S, Zhang J, Venables I, Vanhercke T, Ral JP. Increasing growth and yield by altering carbon metabolism in a transgenic leaf oil crop. Plant Biotechnol J. 2020:**18**(10):2042–2052. https://doi.org/10.1111/pbi.13363

Negi J, Munemasa S, Song B, Tadakuma R, Fujita M, Azoulay-Shemer T, Engineer CB, Kusumi K, Nishida I, Schroeder JI, et al. Eukaryotic lipid metabolic pathway is essential for functional chloroplasts and CO2 and light responses in Arabidopsis guard cells. Proc Natl Acad Sci USA. 2018:**115**(36):9038–9043. https://doi.org/10.1073/pnas.1810458115

Olesinski AA, Lucas WJ, Galun E, Wolf S. Pleiotropic effects of tobacco-mosaic-virus movement protein on carbon metabolism in transgenic tobacco plants. Planta. 1995:**197**(1):118–126. https://doi.org/10.1007/BF00239947

Oparka KJ, Roberts AG, Boevink P, Santa Cruz S, Roberts I, Pradel KS, Imlau A, Kotlizky G, Sauer N, Epel B. Simple, but not branched, plasmodesmata allow the nonspecific trafficking of proteins in developing tobacco leaves. Cell. 1999:**97**(6):743–754. https://doi.org/10.1016/S0092-8674(00)80786-2

Pan R, Liu J, Wang S, Hu J. Peroxisomes: versatile organelles with diverse roles in plants. New Phytol. 2020:**225**(4):1410–1427. https://doi.org/10.1111/nph.16134

Parajuli S, Kannan B, Karan R, Sanahuja G, Liu H, Garcia-Ruiz E, Kumar D, Singh V, Zhao H, Long S, et al. Towards oilcane: engineering hyperaccumulation of triacylglycerol into sugarcane stems. GCB Bioenergy. 2020:**12**(7):476–490. https://doi.org/10.1111/gcbb.12684

Peterson RB. Regulation of Glycine decarboxylase and l-serine hydroxymethyltransferase activities by glyoxylate in tobacco leaf mitochondrial preparations. Plant Physiol. 1982:**70**(1):61–66. https://doi.org/10.1104/pp.70.1.61

Pouvreau B, Vanhercke T, Singh S. From plant metabolic engineering to plant synthetic biology: the evolution of the design/build/test/learn cycle. Plant Sci. 2018:**273**:3–12. https://doi.org/10.1016/j.plantsci.2018.03.035

Pritchard SL, Charlton WL, Baker A, Graham IA. Germination and storage reserve mobilization are regulated independently in Arabidopsis. Plant J. 2002:**31**(5):639–647. https://doi.org/10.1046/j.1365-313X.2002.01376.x

Qaisar U, Akhtar F, Azeem M, Yousaf S. Studies on involvement of Wrinkled1 transcription factor in the development of extra-long staple in cotton. Indian J Genet Plant Breed. 2017:**(2)**:77.

Qu J, Ye J, Geng Y-F, Sun Y-W, Gao S-Q, Zhang B-P, Chen W, Chua N-H (2012) Dissecting functions of *KATANIN* and *WRINKLED1* in cotton fiber development by virus-induced gene silencing. Plant Physiol. **160**(2): 738–748 https://doi.org/10.1104/pp.112.198564

R Core Team. R: a language and environment for statistical computing. Vienna (Austria): R Foundation for Statistical Computing; 2023. https://www.R-project.org/

Regmi A, Shockey J, Kotapati HK, Bates PD. Oil-producing metabolons containing DGAT1 use separate substrate pools from those containing DGAT2 or PDAT. Plant Physiol. 2020:**184**(2):720–737. https://doi.org/10.1104/pp.20.00461

Schwender J, König C, Klapperstück M, Heinzel N, Munz E, Hebbelmann I, Hay JO, Denolf P, De Bodt S, Redestig H, et al. Transcript abundance on its own cannot be used to infer fluxes in central metabolism. Front Plant Sci. 2014:**5**:668. https://doi.org/10.3389/fpls.2014.00668

Shi X, Bloom A. Photorespiration: the futile cycle? Plants. 2021:**10**(5): 908. https://doi.org/10.3390/plants10050908

Singh R, Arora A, Singh V. Biodiesel from oil produced in vegetative tissues of biomass—a review. Bioresour Technol. 2021:**326**:124772. https://doi.org/10.1016/j.biortech.2021.124772

Timm S. The impact of photorespiration on plant primary metabolism through metabolic and redox regulation. Biochem Soc Trans. 2020:**48**(6):2495–2504. https://doi.org/10.1042/BST20200055

Timm S, Bauwe H. The variety of photorespiratory phenotypes—employing the current status for future research directions on photorespiration. Plant Biol. 2013:**15**(4):737–747. https://doi.org/10.1111/j.1438-8677.2012.00691.x

Timm S, Florian A, Arrivault S, Stitt M, Fernie AR, Bauwe H. Glycine decarboxylase controls photosynthesis and plant growth. FEBS Lett. 2012:**586**(20):3692–3697. https://doi.org/10.1016/j.febslet.2012.08.027

Timm S, Florian A, Fernie AR, Bauwe H. The regulatory interplay between photorespiration and photosynthesis. J Exp Bot. 2016:**67**(10): 2923–2929. https://doi.org/10.1093/jxb/erw083

Timm S, Hagemann M. Photorespiration—how is it regulated and how does it regulate overall plant metabolism? J Exp Bot. 2020:**71**(14): 3955–3965. https://doi.org/10.1093/jxb/eraa183

Tjellström H, Strawsine M, Ohlrogge JB. Tracking synthesis and turnover of triacylglycerol in leaves. J Exp Bot. 2015:**66**(5):1453–1461. https://doi.org/10.1093/jxb/eru500

Vanhercke T, Belide S, Taylor MC, El Tahchy A, Okada S, Rolland V, Liu Q, Mitchell M, Shrestha P, Venables I, et al. Up-regulation of lipid biosynthesis increases the oil content in leaves of Sorghum bicolor. Plant Biotechnol J. 2019a:**17**(1):220–232. https://doi.org/10.1111/pbi.12959

Vanhercke T, Divi UK, El Tahchy A, Liu Q, Mitchell M, Taylor MC, Eastmond PJ, Bryant F, Mechanicos A, Blundell C, et al. Step changes in leaf oil accumulation via iterative metabolic engineering. Metab Eng. 2017:**39**:237–246. https://doi.org/10.1016/j.ymben.2016.12.007

Vanhercke T, Dyer JM, Mullen RT, Kilaru A, Rahman MM, Petrie JR, Green AG, Yurchenko O, Singh SP. Metabolic engineering for enhanced oil in biomass. Prog Lipid Res. 2019b:**74**:103–129. https://doi.org/10.1016/j.plipres.2019.02.002

Vanhercke T, El Tahchy A, Liu Q, Zhou X-R, Shrestha P, Divi UK, Ral J-P, Mansour MP, Nichols PD, James CN, et al. Metabolic engineering of biomass for high energy density: oilseed-like triacylglycerol yields from plant leaves. Plant Biotechnol J. 2014:**12**(2):231–239. https://doi.org/10.1111/pbi.12131

Vogel C, Marcotte EM. Insights into the regulation of protein abundance from proteomic and transcriptomic analyses. Nature reviews genetics. 2012:**13**(4):227. https://doi.org/10.1038/nrg3185

Xu C, Shanklin J. Triacylglycerol metabolism, function, and accumulation in plant vegetative tissues. Annu Rev Plant Biol. 2016:**67**(1): 179–206. https://doi.org/10.1146/annurev-arplant-043015-111641

Yang W, Wang G, Li J, Bates PD, Wang X, Allen DK. Phospholipase Dzeta enhances diacylglycerol flux into triacylglycerol. Plant Physiol. 2017:**174**(1):110–123. https://doi.org/10.1104/pp.17.00026

Yu L, Fan J, Yan C, Xu C. Starch deficiency enhances lipid biosynthesis and turnover in leaves. Plant Physiol. 2018:**178**(1):118–129. https://doi.org/10.1104/pp.18.00539

Zhai Z, Keereetaweep J, Liu H, Xu C, Shanklin J. The role of sugar signaling in regulating plant fatty acid synthesis. Front Plant Sci. 2021:**12**:643843. https://doi.org/10.3389/fpls.2021.643843

Zhou XR, Bhandari S, Johnson BS, Kotapati HK, Allen DK, Vanhercke T, Bates PD. Reorganization of acyl flux through the lipid metabolic network in oil-accumulating tobacco leaves. Plant Physiol. 2020:**182**(2):739–755. doi:10.1104/pp.19.00667